metals

MDPI

Article

Simulation of Mechanical Response in Machining of Ti-6Al-4V Based on Finite Element Model and Visco-Plastic Self-Consistent Model

Qingqing Wang [1,*], Chengli Yang [1], Haifeng Yang [1] and Yibo He [2]

[1] School of Mechatronic Engineering, China University of Mining and Technology, Xuzhou 221116, China
[2] State Key Laboratory of Solidification Processing, Center of Advanced Lubrication and Seal Materials, Northwestern Polytechnical University, Xi'an 710072, China
* Correspondence: 5936@cumt.edu.cn

Abstract: The predictions of mechanical responses (stress–strain variations) in the machining of Ti-6Al-4V alloy are important to analyze the deformation conditions of machining to optimize the machining parameters and investigate the generation of a machined surface. The selection of a constitutive model is an essential factor that determines the deformation behavior in the machining simulation model. In this paper, two constitutive models of a modified Johnson–Cook (JC) equation and visco-plastic self-consistent (VPSC) model were used to investigate the stress–strain evolutions in the machining process of Ti-6Al-4V. A finite element (FE) machining model was established, considering the influences of grain refinement and deformation twins, based on a modified JC equation. The VPSC model was fitted based on the macro-strain rate sensitivity of the JC equation. The prediction results of the stress–strain curves of two models were compared, and their validities were further proved. The results show that flow stress hardening and inhomogeneities are caused by multi-scale grain refinement during the machining process of Ti-6Al-4V. Five slip deformation modes and one compressive twinning mode were activated in the VPSC model to be consistent with the macro-deformation behavior predicted with the FE model. The validations show the effectiveness of the modified JC equation, considering microstructural changes and the fitted VPSC model, in predicting dynamic behavior in the machining process of Ti-6Al-4V. The results provide two aspects of macro-deformation and polycrystal plasticity to elucidate the stress variations that occur during the machining of Ti-6Al-4V.

Keywords: machining; stress–strain response; VPSC; JC constitutive; Ti-6Al-4V

check for updates

Citation: Wang, Q.; Yang, C.; Yang, H.; He, Y. Simulation of Mechanical Response in Machining of Ti-6Al-4V Based on Finite Element Model and Visco-Plastic Self-Consistent Model. *Metals* **2023**, *13*, 1362. https://doi.org/10.3390/met13081362

Academic Editor: Hussien Hegab

Received: 29 June 2023
Revised: 16 July 2023
Accepted: 20 July 2023
Published: 28 July 2023

Copyright: © 2023 by the authors. Licensee MDPI, Basel, Switzerland. This article is an open access article distributed under the terms and conditions of the Creative Commons Attribution (CC BY) license (https://creativecommons.org/licenses/by/4.0/).

1. Introduction

Macro-mechanical responses (stress–strain variations), as well as temperature distributions and micro-structural phenomena, occur in the machining process as severe plastic deformations which are imposed on the material [1,2]. For the machining process, investigations focus on the deformation behavior and formation of the machined surface [3]. Clearly, the description of deformation behavior in the machining process is fundamental. It is essential to predict the deformation condition accurately (especially the mechanical response of material) during the machining process.

Many finite element (FE) simulations have been conducted to obtain the deformation behavior of the machining process due to the time efficiency and low cost of FE modeling [4–6]. The selection of a material constitutive model is essential to improve the accuracy of the simulation results. The Johnson–Cook (JC) constitutive equation is one of the most widely used in FE machining simulations [7,8]. Strain hardening, strain rate hardening, and temperature softening are coupled in the model to analyze material flow stress. This is an empirical model, as the parameters of the JC equation are determined to

fit the experimental stress–strain data. In other words, the deformation described in the JC equation is treated as a homogeneous deformation.

Meanwhile, research was carried out to modify the JC equation to coincide with the severe plastic deformation of materials in the machining process. The representative research is the Calamaz-modified JC material model, which includes flow softening at large strains and high temperatures [9]. Hou et al. [10] also modified the JC equation, considering the coupled effects of strain and temperature during the machining process of Ti-6Al-4V alloy. Xu et al. [4], Sima and Özel [6], and Chen et al. [11] also made some improvements in the JC equation in the FE machining simulation model. These modifications typically couple the macroscopic phenomena (such as strain-softening) in the machining process of Ti-6Al-4V. Microstructural evolutions were also detected in the machining process. Their effects on material deformation should be considered in the constitutive model.

Rotella and Umbrello et al. [12] proposed a new material model, considering the effect of grain size, based on the Calamaz-modified JC model. This constitutive equation considers the microstructural phenomena of the control material mechanical response. Another kind of constitutive model is based on the physical phenomena underlying the machining process; for instance, the dislocation-density-based constitutive model [13]. As these studies show, the empirically or phenomenologically based constitutive models implemented in the FE machining model describe the deformations in the workpiece from point to point. The heterogeneous deformations caused by the microstructural features cannot be predicted accurately.

A polycrystal constitutive model was proposed to describe the material point deformation response in the severe deformation process. The stress–strain relationship of material at multiple scales (grain level and macroscopic scale) is provided. The macroscopic deformation is depicted by the microscopic scale deformations in crystallographic slip or twinning systems. Over the years, polycrystal constitutive models, such as the Taylor-type model, visco-plastic self-consistent (VPSC) model, and elasto-VPSC, have been developed to solve the connection of micro to macro [14–17]. Among them, the VPSC model is widely used to predict the heterogeneity in stress–strain variations and textural features in the severe material deformation process. In the VPSC model, the strain rate sensitivity exponent for the microscopic scale (grain level) is usually set independently for the macroscopic deformation. Galán-López and Verleysen [18] simulated the deformation behavior of a Ti-6Al-4V sheet under a range of loading conditions (uniaxial, plane strain, and simple shear) with the VPSC model. The strain rate sensitivity exponent at the microscopic scale was modified based on the strain-rate-hardening term of the JC equation. It was verified that the modified VPSC model can be used to predict the stress–strain variation in a material together with its crystallographic texture.

However, a prerequisite for VPSC simulation is obtaining the velocity gradient in the machining process. It is difficult to obtain the deformation histories via an experiment in the high-strain-rate deformation process [19]. The VPSC simulation must be coupled with the FE model to predict the stress–strain relation from a multi-scale deformation theory. In the present work, a Ti-6Al-4V alloy was selected as the research material. It is a typical two-phase alloy with a large percentage of α phase (>90%) and a small percentage of β phase. Its deformation mainly depends on the α phase of a hexagonal closed packed (HCP) structure. In addition, microstructural changes (grain refinement, nano-twins) are complex during the machining process of the Ti-6Al-4V alloy [20,21]. These changes will further cause material deformation. Therefore, the effects of microstructural changes in the machining process of Ti-6Al-4V should be included in the modified JC constitutive model.

This paper starts with the development of a machining simulation model with Abaqus/Explicit software (6.14, Dassault Systèmes, Paris, France). A modified JC equation introducing the effects of microstructural changes is implemented in the FE model. Then, the strain rate sensitivity exponent of the VPSC model is re-determined according to the modified JC constitutive model. Finally, the stress–strain variations during the machining process ofTi-6Al-4V, predicted with the FE model and VPSC model, are analyzed. The

digital image correlation (DIC) technique coupled with high-speed imaging is used to prove the reliability of the strain field predicted with the modified JC model. The crystallographic texture evolutions of Ti-6Al-4V alloy are also investigated to validate the accuracy of the VPSC model.

2. Experiments and Modeling

2.1. FE Model of the Machining Process of Ti-6Al-4V Alloy

A two-dimensional plain-strain orthogonal machining model for Ti-6Al-4V was developed with arbitrary Lagrangian–Eulerian (ALE) framework. The machining model is shown in Figure 1. A workpiece the size of 2 mm × 1 mm was fixed and the cutting tool was set to move in an opposite direction of X. The cutting tool was assumed to be a rigid body. In the uncut chip region, the mesh element (CPE4RT) size was about 8 μm × 4 μm. The total number of elements in the workpiece was about 32,000. The element size had an influence on the simulation results [4]. The mesh element sizes in the workpiece were determined based on the research of Zhang et al. [22] and Xu et al. [4], in which Lagrangian formulation and a coupled Eulerian–Lagrangian formulation were used in their machining simulation model. A dynamic temperature-displacement explicit step was used in the machining model. Friction between the tool and the chip was defined with a simple Coulomb model [9]. The cutting distance was about 1 mm. The deformation behavior of Ti-6Al-4V was defined with a modified JC constitutive model. A strain-softening effect is considered in the modified JC equation, which is expressed with Equation (1).

$$\sigma = \left[A + B\left(1 + m_1' \ln \frac{T}{T_r}\right)\varepsilon^n\right]\left[1 + C \ln\left(\frac{\dot{\varepsilon}}{\dot{\varepsilon}_0}\right)\right]\left[1 - \left(\frac{T - T_r}{T_m - T_r}\right)^m\right] \quad (1)$$

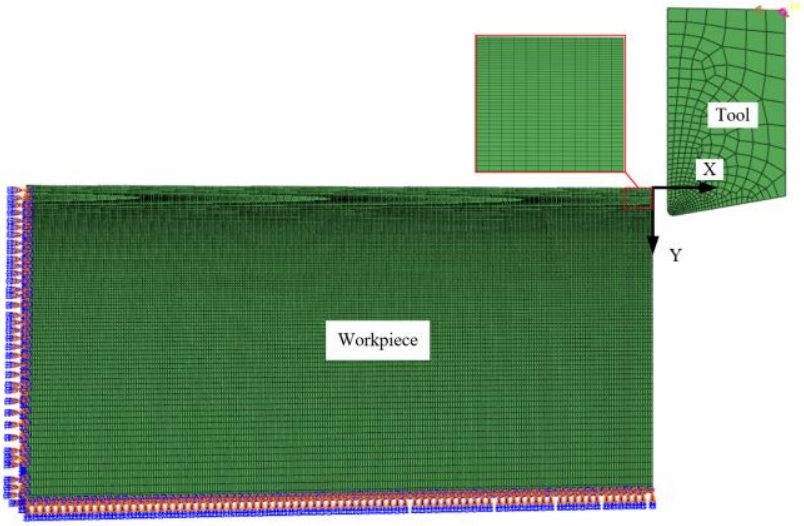

Figure 1. Established machining prediction model.

The JC parameters of A, B, C, n, m_1', and m denote the initial yield stress (920 MPa), strain-hardening modulus (400 MPa), strain-rate-hardening modulus (0.042), strain-rate-hardening exponent (0.578), strain-softening effect (−0.158), and temperature-softening index (0.633), respectively [10]. $\dot{\varepsilon}_0$ is the reference strain rate (0.0001 s^{-1}). T_m is the melting temperature of Ti-6Al-4V (1650 °C). T_r is the ambient temperature (20 °C). According to previous researches, grain refinement and nano-twins are generated during the machining process of Ti-6Al-4V alloy [20,21]. These microstructural changes can cause corresponding hardening effects of Ti-6Al-4V alloy. And the hardening effects are quantitatively estimated via modifying parameter A related to refined grain size (d).

Grain refinement in the machining process of Ti-6Al-4V was predicted using the Zenner–Hollomon (Z-H) dynamic recrystallization model. Grain size (d) is defined as,

$$d = a_1 d_0^{h_1} \varepsilon^{n_1} \left(\dot{\varepsilon} \exp(Q/RT)\right)^{m_1} + c_1 \quad (2)$$

in which Q is the activation energy of Ti-6Al-4V alloy, and its value is 376,000 J·mol^{-1}. R is the gas constant, and its value is 8.3145 J·K^{-1}·mol^{-1}. h_1, m_1, and n_1 represent the influences of initial average grain size (d_0), strain rate, temperature, and strain on the refined grain size, respectively. a_1 and c_1 are two material constants. A critical strain is defined with Equation (3) to control the activation of dynamic recrystallization for Ti-6Al-4V alloy.

$$\varepsilon_{cr} = a_2 d_0^{h_2} \left(\dot{\varepsilon} \exp(Q/RT)\right)^{m_2} + c_2 \quad (3)$$

in which the corresponding constants represent the same physical meanings similar to that in Equation (2). The values of these parameters (a_1, c_1, h_1, m_1, n_1, a_2, c_2, h_2, m_2) in Equations (2) and (3) were calibrated from the experimental data [23].

According to the Hall–Petch (H-P) strength mechanism, parameter A in Equation (1) is modified as $\left(A + k_s d^{-0.5}\right)$ to consider the hardening of grain refinement. The parameter k_s is the H-P strength constant and its value varies with different temperatures [24]. Its noted grain size predicted with the Z-H model is at the micrometer level. The sizes of nano-twins generated in the machining process of Ti-6Al-4V are at the nanometer scale, and their influences on parameter A include two aspects of H-P mechanism and the Basinski hardening mechanism [25,26].

On the one hand, twin boundaries take the role of grain boundaries, and their hardening is defined with the H-P strength equation. On the other hand, the Basinski hardening mechanism of nano-twins is that sliding dislocation in nano-twins transformed into sessile dislocation. When deformation twinning occurred, parameter A could be defined as,

$$\sigma_t = \left[A + k_s d^{-0.5} + k_t d_t^{-0.5}\right] \times \left[1 + (M-1) \times f_t\right] \quad (4)$$

in which σ_t is the work-hardening caused by deformation twins. It includes two aspects of the H-P strengthening mechanism (first bracket) and Basinski hardening mechanism (second bracket). D_t is the effective grain size considering the generation of deformation twinning. K_t is the H-P strengthen coefficient, and its value is the same as k_s. f_t is the twin volume fraction and M is the Basinski hardening effect [26]. The flow stress in the un-twinned region could be expressed with the hardening induced by grain refinement at the meso-scale.

Similarly to the grain refinement model, the occurring of deformation twinning in the machining process is controlled with a critical stress σ_c, which is expressed in terms of the strain rate, temperature, and grain size [27].

$$\sigma_c = K\dot{\varepsilon}^{(-1/m'+1)} \exp\left(Q/\left(m'+1\right)RT\right) + k_c d^{-0.5} \quad (5)$$

where K, m', and k_c are the material parameters. Their values were calibrated according to the variations in the critical stress of twinning activation [23]. Previous researches reported that the deformation twinning type is mainly characterized as $\{10\bar{1}1\}$ twinning in the machining process of Ti-6Al-4V [20,21]. When the flow stress of Ti-6Al-4V in the machining process is larger than σ_c, deformation twinning is formatted. The parameters of K, m', and k_c in Equation (5) were determined as the range of 23 to 25, 16.49, and 18 MPa·mm$^{0.5}$, respectively [23].

Twin volume fraction in the machining process is expressed as,

$$f_t = f \times \tanh\left(\pi \frac{\langle \overline{\sigma} - \sigma_c \rangle}{\sigma_{s'} - \sigma_c}\right) \quad (6)$$

in which the twin volume fraction f_t varies as a hyperbolic tangent function with the increase in flow stress. f is the saturated twin volume fraction and $\sigma_{s'}$ is the corresponding saturated flow stress. The term $\langle \sigma - \sigma_c \rangle$ refers to the relation as follows.

$$\langle \sigma - \sigma_c \rangle = \begin{cases} \sigma - \sigma_c & \sigma \geq \sigma_c \\ 0 & \sigma < \sigma_c \end{cases} \tag{7}$$

The effective grain size d_t, considering the occurrence of deformation twinning, is defined with Equation (8).

$$d_t = (d - d_0) \times \tanh\left(\pi \frac{\langle \sigma - \sigma_c \rangle}{\sigma_{s'} - \sigma_c}\right) + d_0 \tag{8}$$

It is obvious that the generations of deformation twining cause the further refinement of refined grains.

The modified JC model, including grain refinement in meso-scale and nano-twins, was implemented into Abaqus/Explicit via the Vuhard subroutine. The flowchart of the Vuhard subroutine is shown in Figure 2. The parameters in the Z-H prediction model were modified and calibrated by comparing with the experiment results at a certain cutting speed. And then the calibrated parameters were expanded to other cutting conditions. Table 1 gives the calibrated values of the Z-H prediction model for Ti-6Al-4V alloy. To verify the reliability of the established deformation twining prediction model, the prediction results of the twin volume fraction for Ti-6Al-4V in the machining process were compared with the TEM experimental results and the research of Xu et al. [21]. A detailed analysis was conducted in our previous research [23]. Here, only the mechanical response of Ti-6Al-4V in the machining process is concerned.

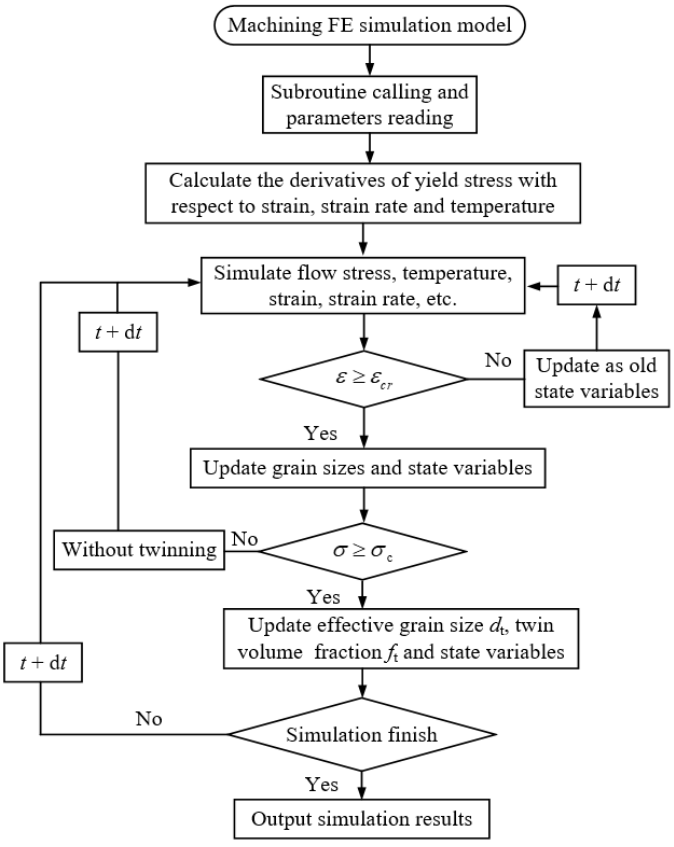

Figure 2. Flowchart of Vuhard.

Table 1. Calibrated parameters of Z-H model for Ti-6Al-4V.

Parameter	a_1	h_1	m_1	n_1	c_1	a_2	h_2	m_2	c_2
Value	1700	0	−0.096	0	0	0.64	0	0.008	0

2.2. VPSC Model to Be Fitted with JC Constitutive Equation

The constitutive model in the grain level of the VPSC model is expressed with a nonlinear rate-dependent equation [16],

$$\dot{\varepsilon}_g = \sum_s m_{ij}^s \gamma^s = \dot{\gamma}_0 \sum_{s=1}^{S} m_{ij}^s \left(\frac{m_{kl}^s \sigma_{kl}}{\tau^s} \right)^{n_s} \tag{9}$$

in which m_{ij}^s is the symmetric Schmid tensor of slip/twinning system s. γ^s is the local shear rate in the slip/twinning system s. n_s means the rate sensitivity exponent. τ^s denotes the critical resolved shear stress of involved slip/twinning systems and it is expressed with the Voce hardening model. Each grain is assumed as an elliptical inclusion embedded in a homogeneous medium (polycrystal). And the constitutive equation at the polycrystal level is obtained based on the single grain constitutive model via the self-consistent method.

In the research of Galán-López and Verleysen [18], n_s is assumed to define the macroscopic strain-rate-hardening effect of Ti-6Al-4V, and its value was re-determined according to the JC equation. Similarly, in this research, the value of n_s was reset based on the modified JC model considering grain refinement at the meso-scale. The stress–strain relation in Equation (9) can be expressed as,

$$\dot{\varepsilon} = \dot{\varepsilon}_0 \left(\frac{\sigma(\dot{\varepsilon})}{\sigma(\dot{\varepsilon}_0)} \right)^{n_s} \tag{10}$$

The strain rate sensitivity proportional factors of $k(\dot{\varepsilon})$ in the VPSC model and $k'(\dot{\varepsilon})$ in the modified JC constitutive model are defined as, respectively,

$$k(\dot{\varepsilon}) = \frac{\sigma(\dot{\varepsilon})}{\sigma(\dot{\varepsilon}_0)} = \left(\frac{\dot{\varepsilon}}{\dot{\varepsilon}_0} \right)^{\frac{1}{n_s}} \tag{11}$$

$$k'(\dot{\varepsilon}) = \frac{\sigma(\dot{\varepsilon})}{\sigma(\dot{\varepsilon}_0)} = \left[A + B \left(1 + m_1' \ln \frac{T}{T_r} \right) \varepsilon^n \right] \left[1 + C \ln \left(\frac{\dot{\varepsilon}}{\dot{\varepsilon}_0} \right) \right] \tag{12}$$

At certain strain and temperature, the variations in the strain rate sensitivity proportional factor under different strain rates would be obtained. The value of the rate sensitivity exponent n_s could be modified according to Equation (12).

It is noted that the strain rate sensitivity proportional factor $k'(\dot{\varepsilon})$ in the original JC constitutive model is simplified as $\left[1 + C \ln \left(\frac{\dot{\varepsilon}}{\dot{\varepsilon}_0} \right) \right]$. However, in the modified JC equation, parameter A includes the influence of grain refinement. And thus the expression of $k'(\dot{\varepsilon})$ becomes complicated. The variations in strain and temperature can also influence the values of $k'(\dot{\varepsilon})$. If the values of strain and temperature were set in the range of deformation conditions that grain refinement occurred, their effects on $k'(\dot{\varepsilon})$ are minor. Figure 3 presents the variations in strain rate sensitivity proportional factors for the VPSC model and the modified JC constitutive model under various strain rates (0.0001–10,000 s^{-1}). The value of n_s is estimated to be about 41, which coincided with the distribution of $k'(\dot{\varepsilon})$ for the modified JC constitutive model with parameter C of 0.042. To illustrate the effects of grain sizes in Equation (12), the variation in $k'(\dot{\varepsilon})$ in the original JC equation was also plotted. It is obvious that a certain hardening is caused by the grain refinement of Ti-6Al-4V alloy which occurred in the machining process. It can also be assumed that the VPSC

model with the calibrated value of n_s can predict the macroscopic deformation behavior of Ti-6Al-4V alloy.

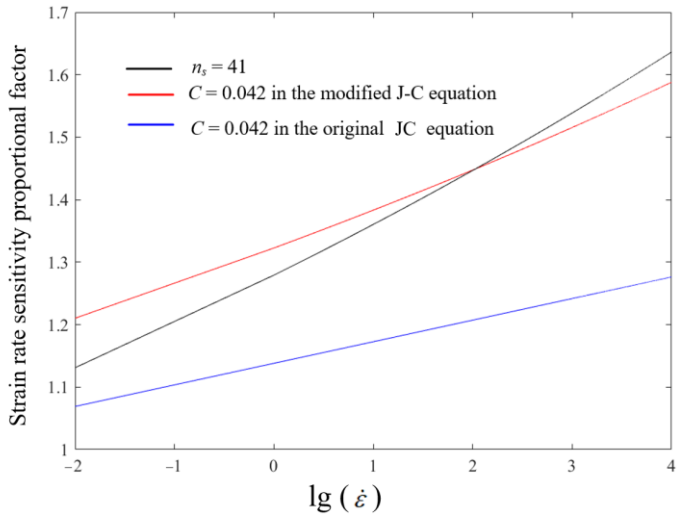

Figure 3. Variations in $k(\dot{\varepsilon})$ in the VPSC model with n_s of about 41, $k'(\dot{\varepsilon})$ in the modified JC equation with C of 0.042, and $k'(\dot{\varepsilon})$ in the original JC equation with C of 0.042 (under certain strain of 0.5 and temperature of 400 °C).

The five slip systems of {10$\bar{1}$0}<11–20} prismatic, {0002}<11$\bar{2}$0> basal, {10$\bar{1}$1}<11$\bar{2}$0> pyramidal <a>, {10$\bar{1}$1}<11$\bar{2}$3> 1st order pyramidal <c+a>, and {11$\bar{2}$2}<11$\bar{2}$3> 2nd order pyramidal <c+a>, as well as the one twinning system of {10$\bar{1}$1}, were considered in the VPSC model. Velocity gradient tensors, input data to the VPSC model, were estimated based on the simulation deformation parameters (strain, strain rate) along a defined path into the chip flow direction. The Voce hardening parameters of the involved slip/twinning systems were referenced from the researches of Galán-López et al. [18,28]. Grain sub-division with a certain aspect ratio was defined in the VPSC model to consider the influence of grain refinement [29]. Some of the hardening parameters were further fitted to coincide with the macroscopic deformation condition of Ti-6Al-4V alloy as the influence of a high cutting temperature on the Voce hardening law is ignored. The Voce hardening distributions of the involved slip/twinning systems are presented in Figure 4.

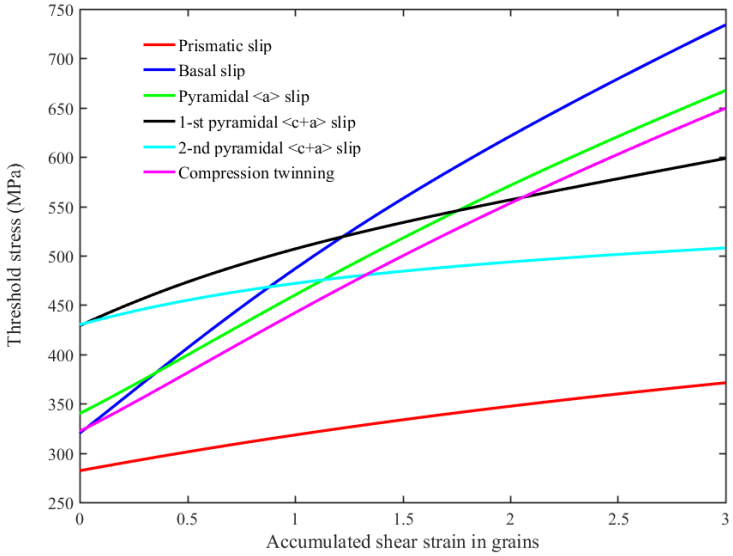

Figure 4. Threshold stress evolutions of different deformation modes (Color online).

2.3. Machining Tests and Microstructure Characterizations

Machining tests provided in [23] were performed to calibrate the modified JC equation while considering microstructural changes. Here, only a simple description was presented to repeat the cutting conditions. Five kinds of cutting speeds ranging from 100 m/min to 500 m/min with an interval of 100 m/min were used in the machining experiments. The feed rate was set to a constant of 0.1 mm/z. The cutting tool is the cemented carbide uncoated material (WC-6%Co). The insert type is NG3125R K313, Kennametal. The back angle of the cutting insert is about 6–7°. The tool rake angle is 0°. Additional machining experiments were conducted to verify the prediction results of deformation histories (strain, strain rate) for the established FE model and VPSC model.

The experiment setup is shown in Figure 5. High-speed imaging coupled with DIC tests were performed to obtain the deformation fields of Ti-6Al-4V in the machining process. The camera was positioned at a mobile platform, with 3 directions stationed on the lathe perpendicular to the end face of the workpiece. A microscope was implemented on the camera to capture the deformation behavior in the primary shear zone. The Photron FASTCAM SA-Z camera with a maximum frame rate of 20,000 s^{-1} was used. An LED lamp was also added in the front of the magnification microscope lens to ensure that more light can enter into the images. Uniformly distributed speckles were made on the end face of the workpiece with high-pressure spray to present the deformation information in the machining process. The subset is 125 × 125 and the step size is 1 pixel. The strain/strain rate fields in the primary shear zone during the machining process were analyzed with VIC-2D Image Correlation Software (Correlated Solutions, Inc., Irmo, SC, USA).



Figure 5. Experimental setup of high-speed imaging. (**a**) Photo of experimental setup; (**b**) photo of primary shear zone.

3. Prediction Results

3.1. Stress–Strain Curves Predicted with FE Model

Figure 6 shows the evolution of the flow stresses of Ti-6Al-4V alloy in the machining process. Intense stresses are imposed to the primary shear zone and the top layer of the machined surface. Chip morphologies cannot be predicted accurately as ALE framework was applied in the FE model. From the perspective of macroscopic deformation, the flow stress distribution can be attributed to the large strain and high strain rate concentrated in the primary shear zone and near to the top surface. Grain refinement in meso-scale and the formation of nano-twins are the microscopic factors that cause inhomogeneous distributions of flow stresses in the machining process. Deformation paths were defined along the chip flow direction (Figure 6a). Deformation histories along defined paths were extracted from the FE model, and the stress–strain evolutions were plotted in Figure 7. The flow stresses of Ti-6Al-4V alloy in the machining process are basically increased with the increase in the cutting speeds. These are consistent with the microstructural changes formatted during the machining process. The maximum flow stress varies from 1300 MPa to 1650 MPa with the increase in cutting speeds. The flow stress under a cutting speed of

400 m/min is a little larger than that under a cutting speed of 500 m/min. This is related to the grain refinement degree and the inhomogeneous distribution of deformation twinning. It is reported that grain refinement degrees in meso-scale present an inflexion because the strain rate and cutting temperature are increased with the increase in the cutting speeds and act as essential roles in determining grain sizes [12,30,31]. Generations of nano-twins under higher cutting speeds further improve the working hardening effects of Ti-6Al-4V and cause the inhomogeneous distributions of flow stresses at higher cutting speeds.

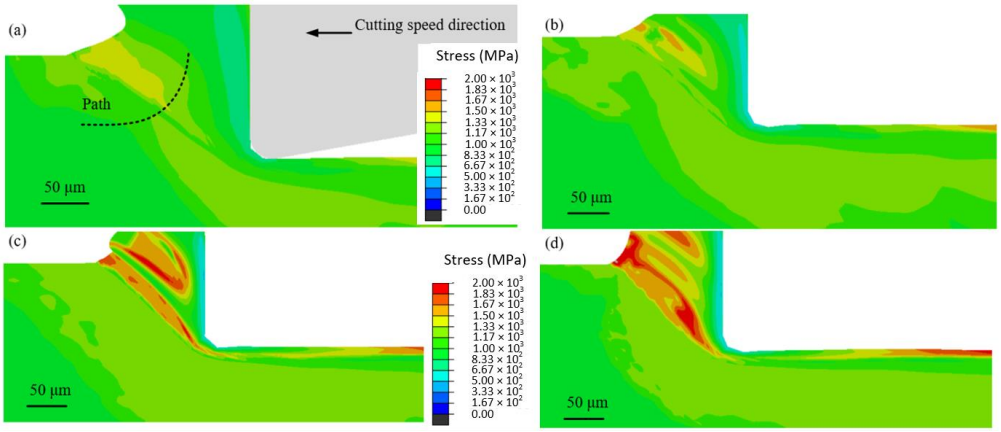

Figure 6. Prediction results of stress map for Ti-6Al-4V in the machining process. (**a**) At cutting speed of 100 m/min; (**b**) at cutting speed of 200 m/min; (**c**) at cutting speed of 400 m/min; (**d**) at cutting speed of 500 m/min.

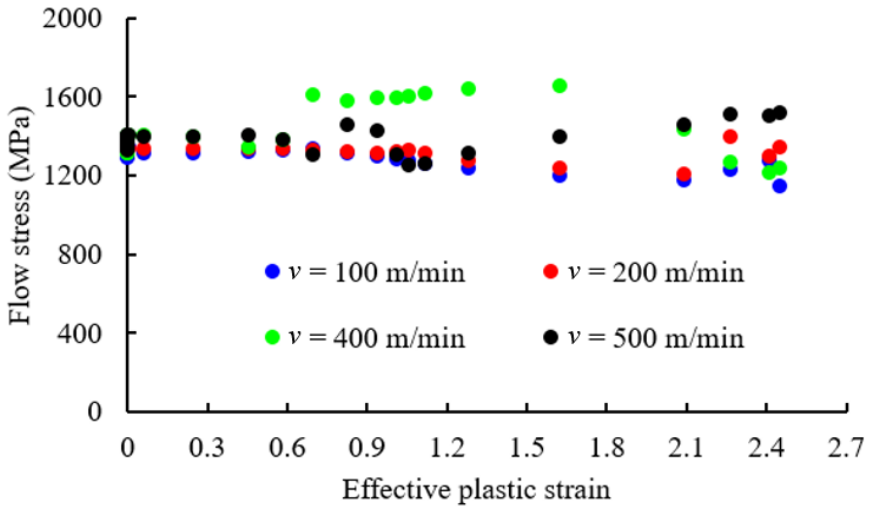

Figure 7. Stress–strain curves of defined paths at different cutting speeds.

To highlight the hardenings of microstructural evolutions in the machining process, an FE machining model without considering grain refinement was established. Figure 8 shows the stress variations for Ti-6Al-4V alloy during the machining process. It is obvious that a relatively uniform deformation is located in the primary shear zone compared with that in Figure 6a,c. The modified JC equation presents the strain-softening, i.e., a strong correlation exists between the strain hardening rate and temperature in the machining process of Ti-6Al-4V alloy [10,11]. And the strain hardening rate decreases with the increase in the cutting temperature. On the other hand, strain rate sensitivity is evident in the dynamic deformation process of Ti-6Al-4V alloy [32,33]. Therefore, there is no apparent increase in the stress at a cutting speed of 400 m/min compared with that at a cutting speed of 100 m/min as a high cutting temperature is generated with the increase in the cutting speed.

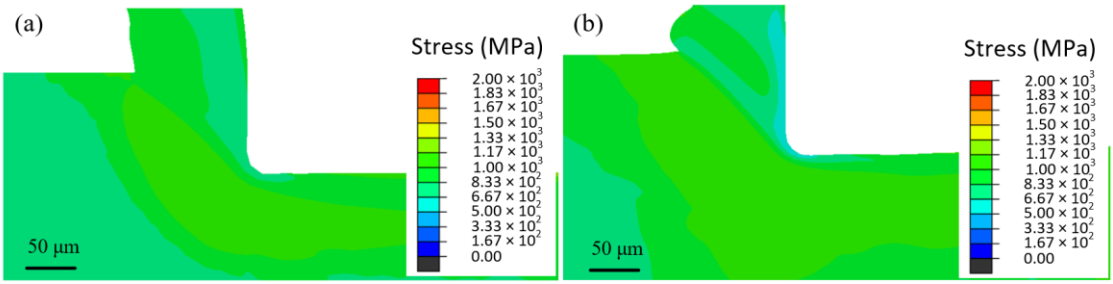

Figure 8. Stress maps predicted with the modified JC equation without considering microstructural changes. (**a**) At cutting speed of 100 m/min; (**b**) at cutting speed of 400 m/min.

3.2. Stress–Strain Variations Predicted with VPSC Model

The deformation conditions of defined paths, as shown in Figure 6a, were extracted from the FE model. Two deformation conditions with/without considering microstructural changes are compared in the VPSC model. Stress–strain evolutions predicted with the VPSC model are plotted in Figure 9. For the deformation conditions with considering microstructural changes, a certain degree of hardening (15–25%) under the same cutting speed is observed. Meanwhile, a large range of increment of flow stress is presented with the increase in the cutting speed. The occurring of grain refinement and deformation twins at higher cutting speed induces hardening. For the deformation data based on the original modified JC model (without considering microstructural changes), the stress shows a little variation with the increase in the cutting speed. This trend is identical with the FE simulation results (Figure 8). It is also proved that the simulation results of the VPSC model are reliable by comparing the stress–strain variations between Figures 7 and 9.

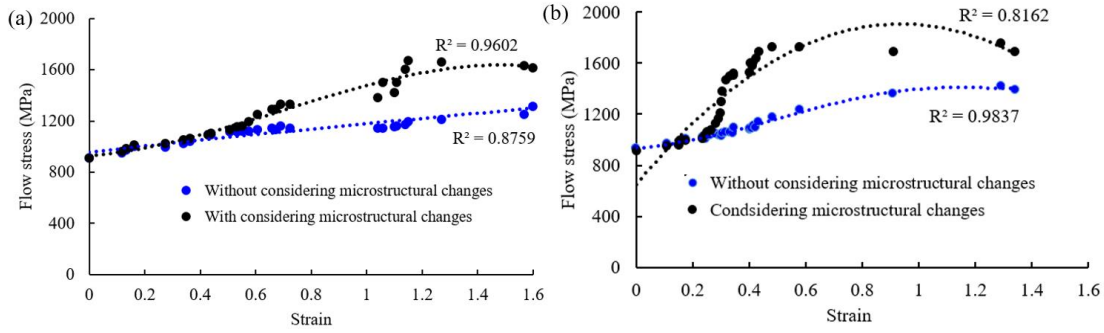

Figure 9. Stress–strain curves predicted with VPSC model. (**a**) At cutting speed of 100 m/min; (**b**) at cutting speed of 400 m/min.

4. Discussion

4.1. Comparisons of FE Model and VPSC Model

As shown in Figure 10, the compared results of flow stresses predicted with the FE model and VPSC model at cutting speeds of 100 m/min and 400 m/min are presented. In the FE simulation model, peak flow stress is located in the primary shear zone. It is because large degrees of grain refinement and twin volume fractions occur in the primary shear zone by comparing that of its nearby zones. However, as seen in Figure 10a, the peak value of flow stress (about 1300 MPa) predicted with the FE model is relatively lower than that of the VPSC model (about 1600 MPa). One reason is that only the influence of grain refinement at the meso-scale is considered in the modified JC model at a lower cutting speed. Another reason can be explained from the perspective of temperature-dependent hardening in the machining process. As described in Equation (1), the strain hardening rate decreases with the increment of cutting temperature. Flow-softening is more severe than that of the nearby zones of the primary shear zone because much heat is imposed into the primary shear zone. Moreover, a Voce hardening model coupling the influence

of temperature should be developed for the VPSC model to accurately predict the flow stresses of Ti-6Al-4V at high-temperature deformation conditions. According to the above discussions, it is logical that a relatively large deviation (about 20%) of flow stresses for Ti-6Al-4V under a low cutting speed predicted with the FE model and VPSC model exists.

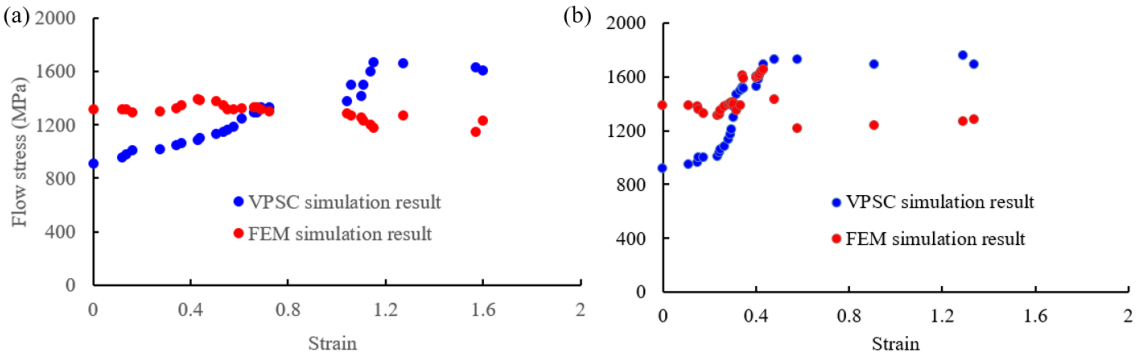

Figure 10. Comparisons of stress–strain variations predicted with FE model and VPSC model. (**a**) At cutting speed of 100 m/min; (**b**) at cutting speed of 400 m/min.

A small difference (6%) of the peak values of flow stresses for two models is seen in Figure 10b. In this condition, the hardening effect of deformation twinning in micro-scale is considered in the modified JC model. Five slip systems as well as compression twinning are assumed to be activated in the VPSC model. The identical prediction results of these two models provide two explanations of the deformation mechanism for Ti-6Al-4V during the machining process. Similarly, stresses predicted with the FE model are decreased in the flow direction of primary shear zones. This is because much more heat is dissipated into the chip flow direction (defined path) and thus caused flow stress softening. It is also noted in Figure 6c that shear bands are prominent at higher cutting speeds. At the end stage of a deformation path, it would be defined outside the shear band in which microstructural changes are little. Hence, the flow stresses predicted with the FE model decrease in the end stage of defined deformation paths.

4.2. Validities of Modified JC Equation and VPSC Model

Plastic strain between FE prediction and DIC measured is compared to validate the accuracy of the FE model with the modified JC equation. Figure 11 shows the distribution of plastic strain in the primary shear zone. The displacements of speckles sprayed in the workpiece were difficult to track under a high strain rate (cutting speed) and small feed rate [19,34]. A representative case (cutting speed is 60 m/min and feed rate is 0.3 mm/r) was selected to obtain the DIC analysis result. As seen in Figure 11b, one serrated chip segment contains a shear band and a bulk segment zone. Equivalent plastic strain increases within the generation of a shear band and gradually ceases to a constant once the shear band is formed. This constant value is the total strain imposed into the primary shear zone. In the prediction strain distribution map (Figure 11a), it is also obvious that strain increases rapidly within a formation of one serrated chip. The serrated chip morphologies show a large difference from the high-speed image as the ALE algorithm was used in the FE prediction model [4]. However, the formations of shear bands for chips can be simulated, and the prediction total strains can be used as references to characterize the deformation histories of Ti-6Al-4V during the machining process. The average plastic strain (about two) in the shear band predicted with the FE model coincides with the DIC analysis result (Sections 2.1–2.3). The predicted deviation of the established FE model is within 15%. This indirectly proves that the established machining simulation model with a modified JC equation is reliable.

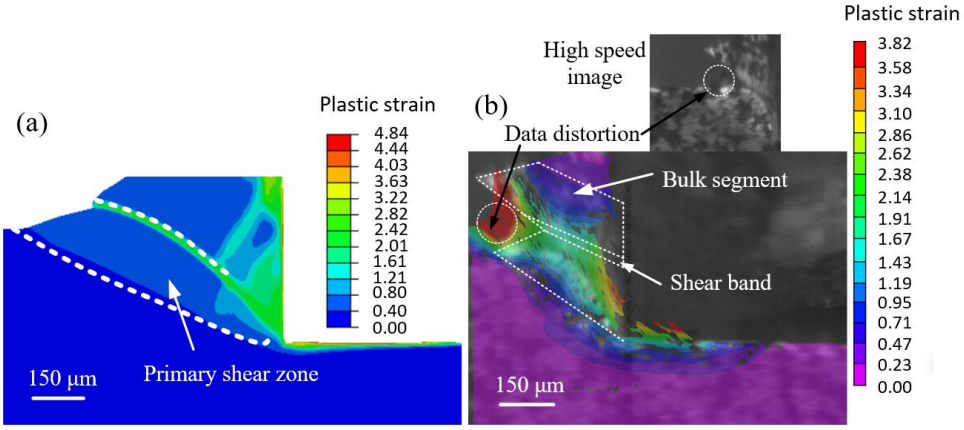

Figure 11. Comparison of plastic strain between FE simulation result and DIC measurement at cutting speed of 60 m/min as well as a large feed rate of 0.3 mm/r. (**a**) FE simulation result; (**b**) DIC analysis result.

The split Hopkinson pressure bar (SHPB) test result, performed in a previous work, is presented to illustrate the prediction stress–strain variation with the VPSC model. The comparison result is seen in Figure 12. The strain rate of the SHPB test was 6000 s^{-1}. In the VPSC model, the deformation condition of the SHPB test was simplified as a uniaxial compression. Only five slip systems of Ti-6Al-4V alloy were considered to be activated in the dynamic compression process. It is seen that flow stress is increased continuously with the increase in the strain as the elastic regime is neglected in the VPSC model [35].

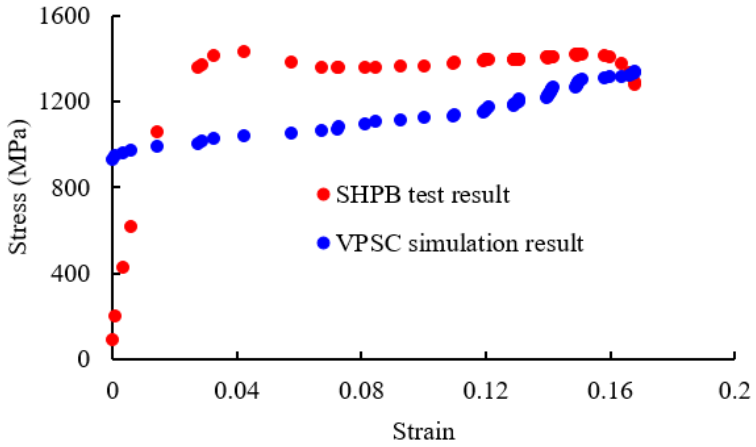

Figure 12. Comparison of the SHPB test and the VPSC simulation at certain strain rate of 6000 s^{-1}.

In the plastic deformation stage, there is a discrepancy in the yield stress of Ti-6Al-4V between the VPSC model and SHPB test. It is because the deformation condition of the SPHB test is simplified in the VPSC model. Actually, shear deformation was observed in the SHPB test of Ti-6Al-4V [36,37]. The average plastic stress obtained with the VPSC model basically coincides with (prediction deviation is about 10%) that in the SHPB test. It is compelling that the calibrated VPSC model can predict the dynamic behavior of Ti-6Al-4V in the machining process.

To further verify the fitted VPSC model, crystallographic texture variations for the Ti-6Al-4V alloy are analyzed. The crystallographic texture characterization of the chip root at a cutting speed of 100 m/min is presented in Figure 13. The inverse pole figure (IPF) map shows that grains are elongated and refined in the primary shear zone of the chip root. A part of the grains is hardly indexed as the severe deformation imposed into the machining process. Corresponding texture variations are presented in pole figures (PFs). A typical C fiber shear texture is formed in the Ti-6Al-4V chip root [38]. Prediction PFs

in Figure 13c also present that the same crystallographic texture is generated. Both the predictions of mechanical response and crystallographic texture of Ti-6Al-4V alloy show that the calibrated VPSC model is reliable to be used in the machining process.

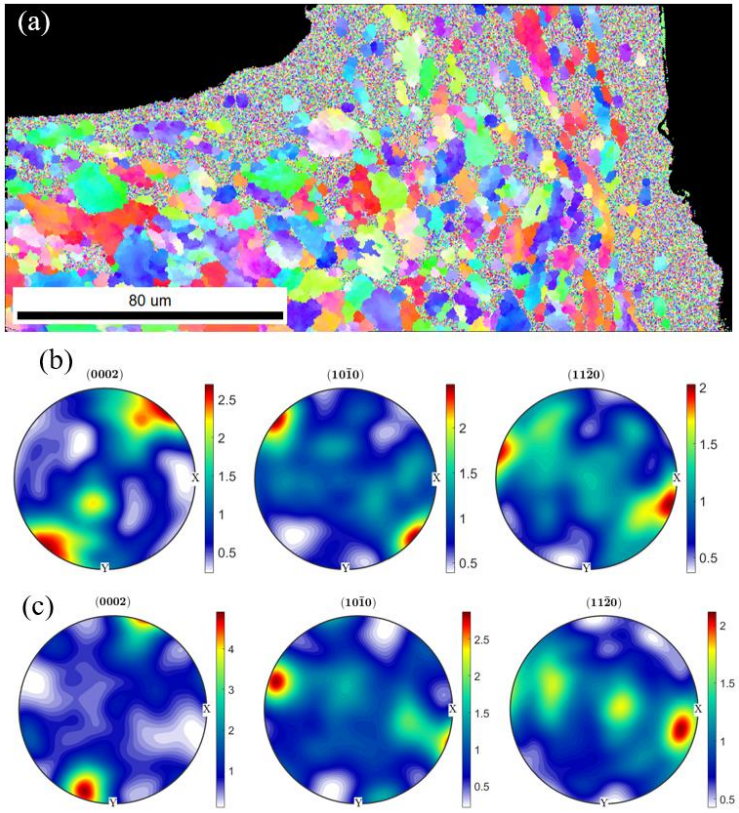

Figure 13. Crystallographic texture variation in Ti-6Al-4V chip root. (**a**) IPF map of Ti-6Al-4V chip root; (**b**) measured PFs; (**c**) predicted PFs.

5. Conclusions

In this study, two methods of an FE model considering grain refinement in multi-scales and a calibrated VPSC model based on macro strain rate sensitivity were presented to describe the stress–strain variations in Ti-6Al-4V alloy during the machining process. FE predictions show that flow stresses are basically increased (peak value varies from 1300 MPa to 1650 MPa) with the cutting speeds ranging from 100 m/min to 500 m/min. Grain refinement at the meso-scale is the hardening mechanism under low cutting speeds (100–200 m/min). And the hardenings at higher cutting speeds are caused by the grain refinement at multiple scales. Moreover, inhomogeneous hardenings are imposed into the primary deformation zone.

Corresponding to the grain refinements at the meso-scale, only slip systems were activated in the VPSC model to simulate the mechanical responses during the machining process of Ti-6Al-4V. The maximum stresses at low cutting speeds predicted with the FE model show an average deviation of about 20% from that with the VPSC model because of the strain-softening effect and micro-hardening mechanism. Five slip systems and one compressive twinning system were activated at higher cutting speeds to be identical with the macro-deformation behavior simulated with the FE model. The flow stresses at higher cutting speeds predicted with the FE model show good agreement (prediction deviation is about 6%) with that of the VPSC model. The DIC analysis of the strain field and crystallographic texture analysis further prove the capability of describing mechanical responses with the FE model and VPSC model in the machining of Ti-6Al-4V alloy. The prediction results reveal the mechanical responses during the machining of Ti-6Al-4V based on macro-mechanics and polycrystal plasticity theory.

Author Contributions: Q.W.: software, validation, investigation, writing—original draft preparation, writing—review and editing; C.Y.: writing—original draft preparation, writing—review and editing; H.Y.: guidance of formal analysis, supervision, writing—review and editing and English writing; Y.H.: supervision, writing—review and editing and English writing. All authors have read and agreed to the published version of the manuscript.

Funding: This research was funded by Natural Science Foundation of China grant number [52105494 and 52275224], Natural Science Foundation of Jiangsu Province for Youths grant number [BK20200640], Chinese Postdoctoral Science Foundation grant number [2019M661976] and the State Key Laboratory of Solidification Processing in NWPU grant number [SKLSP202324]. And The APC was funded by [52105494].

Data Availability Statement: Data are contained within the article.

Conflicts of Interest: The authors declare no conflict of interest.

References

1. Haddag, B.; Yameogo, D.; Nouari, M.; Makich, H. Multi-Physics Analysis of Machining Ti-6Al-4V Alloy: Experimental Characterization and a New Material Behavior Modeling. *Metals* **2022**, *12*, 581.
2. Zhang, J.; Xu, X.; Outeiro, J.; Liu, H.G.; Zhao, W.H. Simulation of Grain Refinement Induced by High-Speed Machining of OFHC Copper Using Cellular Automata Method. *J. Manuf. Sci. Eng.-Trans. ASME* **2020**, *142*, 91006.
3. Liao, Z.R.; La, M.A.; Murray, J.; Speidel, A.; Ushmaev, D.; Clare, A.; Axinte, D.; M'Saoubi, R. Surface Integrity in Metal Machining—Part I: Fundamentals of Surface Characteristics and Formation Mechanisms. *Int. J. Mach. Tools Manuf.* **2021**, *162*, 103687.
4. Xu, X.; Outeiro, J.; Zhang, J.; Xu, B.B.; Zhao, W.H.; Astakhov, V. Machining Simulation of Ti6Al4V Using Coupled Eulerian-Lagrangian Approach and a Constitutive Model Considering the State of Stress. *Simul. Model. Pract. Theory* **2021**, *110*, 102312.
5. Karpat, Y. Temperature dependent flow softening of titanium alloy Ti6Al4V: An investigation using finite element simulation of machining. *J. Mater. Process. Technol.* **2011**, *211*, 737–749.
6. Sima, M.; Özel, T. Modified Material Constitutive Models for Serrated Chip Formation Simulations and Experimental Validation in Machining of Titanium Alloy Ti-6Al-4V. *Int. J. Mach. Tools Manuf.* **2010**, *50*, 943–960.
7. Storchak, M.; Rupp, P.; Möhring, H.C.; Stehle, T. Determination of Johnson–Cook constitutive parameters for cutting simulations. *Metals* **2019**, *9*, 473.
8. Thornton, E.-L.; Zannoun, H.; Vomero, C.; Caudill, D.; Schoop, J. A Review of Constitutive Models and Thermal Properties for Nickel-Based Superalloys Across Machining-Specific Regimes. *J. Manuf. Sci. Eng.-Trans. ASME* **2023**, *145*, 080801.
9. Calamaz, M.; Coupard, D.; Girot, F. A New Material Model for 2D Numerical Simulation of Serrated Chip Formation When Machining Titanium Alloy Ti-6Al-4V. *Int. J. Mach. Tools Manuf.* **2008**, *48*, 275–288.
10. Hou, X.; Liu, Z.Q.; Wang, B.; Lv, W.Y.; Liang, X.L.; Hua, Y. Stress-Strain Curves and Modified Material Constitutive Model for Ti-6Al-4V over the Wide Ranges of Strain Rate and Temperature. *Materials* **2018**, *11*, 938. [PubMed]
11. Chen, G.; Ren, C.Z.; Qin, X.D.; Li, J. Temperature Dependent Work Hardening in Ti-6Al-4V Alloy Over Large Temperature and Strain Rate Ranges: Experiments and Constitutive Modeling. *Mater. Des.* **2015**, *83*, 598–610.
12. Rotella, G.; Umbrello, D. Finite Element Modeling of Microstructural Changes in Dry and Cryogenic Cutting of Ti6Al4V Alloy. *CIRP Ann.-Manuf. Technol.* **2014**, *63*, 69–72.
13. Ding, H.T.; Shin, Y.C. Dislocation Density-Based Grain Refinement Modeling of Orthogonal Cutting of Titanium. *J. Manuf. Sci. Eng.-Trans. ASME* **2014**, *136*, 041003.
14. Kalidindi, S.R.; Bronkhorst, C.A.; Anand, L. Crystallographic Texture Evolution in Bulk Deformation Processing of FCC Metals. *J. Mech. Phys. Solids* **1992**, *40*, 537–569.
15. Taylor, G.I. Plastic Strain in Metals. *J. Inst. Met.* **1938**, *62*, 307–324.
16. Lebensohn, R.A.; Tomé, C. A Self-consistent Anisotropic Approach for the Simulation of Plastic Deformation and Texture Development of Polycrystals: Application to Zirconium Alloys. *Acta Mater.* **1993**, *41*, 2611–2624.
17. Wang, H.; Wu, P.D.; Wang, J.; Tome, C.N. A Crystal Plasticity Model for Hexagonal Close Packed (HCP) Crystals Including Twinning and De-twinning Mechanisms. *Int. J. Plast.* **2013**, *49*, 36–52. [CrossRef]
18. Galán-López, J.; Verleysen, P. Simulation of the Plastic Response of Ti-6Al-4V Thin Sheet under Different Loading Conditions Using the Viscoplastic Self-consistent Model. *Mater. Sci. Eng. A* **2018**, *712*, 1–11.
19. Davis, B.; Dabrow, D.; Ifju, P.; Xiao, G.X.; Liang, S.Y.; Huang, Y. Study of the Shear Strain and Shear Strain Rate Progression During Titanium Machining. *J. Manuf. Sci. Eng.-Trans. ASME* **2018**, *140*, 051007. [CrossRef]
20. Wang, Q.Q.; Liu, Z.Q. Plastic Deformation Induced Nano-scale Twins in Ti-6Al-4V Machined Surface with High Speed Machining. *Mater. Sci. Eng. A* **2016**, *675*, 271–279. [CrossRef]
21. Xu, X.; Zhang, J.; Liu, H.G.; He, Y.; Zhao, W.H. Grain Refinement Mechanism Under High Strain-rate Deformation in Machined Surface During High Speed Machining Ti6Al4V. *Mater. Sci. Eng. A* **2019**, *752*, 167–179.

22. Zhang, Y.; Mabrouki, T.; Nelias, D.; Gong, Y. FE-model for Titanium Alloy (Ti-6Al-4V) Cutting Based on the Identification of Limiting Shear Stress at Tool-chip Interface. *Int. J. Mater. Form.* **2011**, *4*, 11–23.
23. Wang, Q.Q.; Liu, Z.Q.; Cheng, Y.H.; Tian, X.H. Hardness Prediction of TC4 Machined Surface Based on the Evolution of Multi-scale Grain Refinement. *J. S. China Univ. Technol. (Nat. Sci. Ed.)* **2023**, *51*, 35–46.
24. Kim, J.H.; Semiatin, S.; Lee, Y.H.; Lee, C.S. A Self-consistent Approach for Modeling the Flow Behavior of the Alpha and Beta Phases in Ti-6Al-4V. *Metall. Mater. Trans. A* **2011**, *42*, 1805–1814.
25. Basinski, Z.; Szczerba, M.; Niewczas, M.; Embury, J.; Basinski, S. The Transformation of Slip Dislocations During Twinning of Copper-aluminum Alloy Crystals. *Rev. Met.* **1997**, *94*, 1037–1044.
26. Salem, A.; Kalidindi, S.; Semiatin, S. Strain Hardening Due to Deformation Twinning in α-titanium: Constitutive Relations and Crystal-plasticity Modeling. *Acta Mater.* **2005**, *53*, 3495–3502.
27. Meyers, M.A.; Benson, D.J.; Vohringer, O.; Kad, B.K.; Xue, Q.; Fu, H.H. Constitutive Description of Dynamic Deformation: Physically-based Mechanisms. *Mater. Sci. Eng. A* **2002**, *322*, 194–216.
28. Yang, H.P.; Wang, Y.M. Analysis of Deformation and Texture Gradient in Shot Peened Pure Titanium. *IOP Conf. Ser. Mater. Sci. Eng.* **2018**, *409*, 012017.
29. Basu, S.; Ravi, S.M. Crystallographic Textures Resulting From Severe Shear Deformation in Machining. *Metall. Mater. Trans. A* **2015**, *46*, 801–812.
30. Liu, G.; Zhang, D.; Yao, C. Investigation of the Grain Refinement Mechanism in Machining Ti-6Al-4V: Experiments and Simulations. *J. Manuf. Process.* **2023**, *94*, 479–496.
31. Ding, H.; Shen, N.; Shin, Y.C. Modeling of Grain Refinement in Aluminum and Copper Subjected to Cutting. *Comp. Mater. Sci.* **2011**, *50*, 3016–3025. [CrossRef]
32. Fourest, T.; Bouda, P.; Fletcher, L.C.; Notta-Cuvier, D.; Markiewicz, E.; Pierron, F.; Langrand, B. Image-Based Inertial Impact Test for Characterization of Strain Rate Dependency of Ti6Al4V Titanium Alloy. *Exp. Mech.* **2020**, *60*, 235–248.
33. Hu, H.Z.; Xu, Z.J.; Dou, W.; Huang, F.L. Effects of Strain Rate and Stress State on Mechanical Properties of Ti-6Al-4V Alloy. *Int. J. Impact Eng.* **2020**, *145*, 103689.
34. Cai, S.L.; Chen, Y.; Ye, G.G.; Jiang, M.Q.; Wang, H.Y.; Dai, L.H. Characterization of the Deformation Field in Large-Strain Extrusion Machining. *J. Mater. Process. Technol.* **2015**, *216*, 48–58.
35. Zecevic, M.; Knezevic, M.; Beyerlein, I.J.; Tome, C.N. An Elasto-Plastic Self-consistent Model with Hardening Based on Dislocation Density, Twinning and De-twinning: Application to Strain Path Changes in HCP Metals. *Mater. Sci. Eng. A* **2015**, *638*, 262–274.
36. Lee, W.S.; Lin, C.F. Plastic Deformation and Fracture Behaviour of Ti-6Al-4V Alloy Loaded with High Strain Rate Under Various Temperatures. *Mater. Sci. Eng. A* **1998**, *241*, 48–59.
37. Liu, X.; Tan, C.; Zhang, J.; Wang, F.; Cai, H. Correlation of Adiabatic Shearing Behavior with Fracture in Ti-6Al-4V Alloys with Different Microstructures. *Int. J. Impact Eng.* **2009**, *36*, 1143–1149.
38. Wang, Q.Q.; Shankar, R.M.; Liu, Z.Q. Visco-plastic Self-consistent Modeling of Crystallographic Texture Evolution Related to Slip Systems Activated During Machining Ti-6AL-4V. *J. Alloys Compd.* **2021**, *853*, 157336.

Disclaimer/Publisher's Note: The statements, opinions and data contained in all publications are solely those of the individual author(s) and contributor(s) and not of MDPI and/or the editor(s). MDPI and/or the editor(s) disclaim responsibility for any injury to people or property resulting from any ideas, methods, instructions or products referred to in the content.